Article

A greening Earth has reversed the trend of decreasing carbonate weathering under a warming climate

Sibo Zeng [1,5] ✉, Zaihua Liu [2,3,5] ✉, Yongjun Jiang [1], Nico Goldscheider [4], Yan Yang [1], Min Zhao [2], Hailong Sun [2], Haibo He [2], Mingyu Shao[2] & Liangxing Shi [2]

The response of mineral weathering and its related Weathering Sink for atmospheric CO_2 ($WS_{atm\text{-}CO2}$) to global vegetation greening are not well understood. After applying different biogeochemical models and a field experiment to investigate the influence of vegetation greening and warming on the variations of carbonate weathering and $WS_{atm\text{-}CO2}$ on regional and global scales, here we show a significant positive relationship between global carbonate weathering intensity ($[HCO_3^-]$ as a proxy) and vegetation greenness. During 1982–2018, under a warming climate, $[HCO_3^-]$ and $WS_{atm\text{-}CO2}$ increase by 5.8% and 6.1%, respectively, due to vegetation greening, in the carbonate areas of Southwest China. Meanwhile, the $[HCO_3^-]$ in global carbonate areas increases by +2.4% during the same period. By contrast, the $[HCO_3^-]$ in global carbonate areas decreases by −1.3% without a vegetation function due to the warming. Moreover, we estimated that the carbonate weathering enhancements due to vegetation restoration at the global scale could reach 43.8%. Our results demonstrate that future vegetation restoration is important for the carbon capture by mineral weathering.

Mineral weathering is an atmospheric CO_2 capture mechanism[1]. This geologic process can balance the global warming caused by human greenhouse gas emissions in the short term, or the greenhouse gas emissions from volcanism on geologic time scales[1-3]. The chemical weathering of carbonate is rapid and provides significant carbon capture within a geologically short intreval[3,4]. Through the dissolution of carbonate minerals by carbonic acid (calcite is an example), the atmospheric CO_2 or soil CO_2 (of atmospheric origin) at the soil-rock interface can be converted to dissolved inorganic carbon (DIC) in inland waters, which generates an atmospheric CO_2 sink[5]. In a natural water-pH environment, the major form of DIC is bicarbonate (HCO_3^-). Thus, this geologic process can be expressed using the following simplified equation[2]:

$$CaCO_3 + CO_2 + H_2O = Ca^{2+} + 2HCO_3^- \quad (1)$$
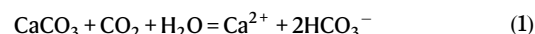
In a pure carbonate system, the greater the carbonate dissolution the greater the HCO_3^- production (atmospheric CO_2 capture). Hence, the concentration of bicarbonate ($[HCO_3^-]$) in the aquifers of carbonate-dominated catchments can be viewed as a proxy of carbonate weathering intensity and atmospheric CO_2 capture capacity. The state of global carbonate weathering has changed substantially in the modern era. During the past few decades, increases in carbonate

[1]Chongqing Key Laboratory of Karst Environment & School of Geographical Sciences of Southwest University, Chongqing, China. [2]State Key Laboratory of Environmental Geochemistry (SKLEG), Institute of Geochemistry, Chinese Academy of Sciences (CAS), Guiyang, China. [3]CAS Center for Excellence in Quaternary Science and Global Change, Xi'an, China. [4]Institute of Applied Geosciences, Division of Hydrogeology, Karlsruhe Institute of Technology (KIT), Karlsruhe, Germany. [5]These authors jointly supervised this work: Sibo Zeng, Zaihua Liu. ✉e-mail: swsibozeng@swu.edu.cn; liuzaihua@vip.gyig.ac.cn

weathering intensity ([HCO$_3^-$] as a proxy) and the weathering sink for atmospheric CO$_2$ ($WS_{\text{atm-CO2}}$) have been detected in major rivers and carbonate aquifers worldwide[6–9]. The striking variations in carbonate weathering between different regions are thought to be related to ongoing global changes, including rising atmospheric CO$_2$ and temperature, changes in runoff, and land-use dynamics[6,8,10–12]. However, previous studies typically employed statistical methods for data analysis, and our current understanding of the quantitative relationships between carbonate weathering and its potential drivers, and the inherent mechanisms governing variations in carbonate weathering under global climate change, are lacking. While the sensitive response of carbonate weathering to global change has been detected by the scientific community, how it has increased during the past few decades and how humans can promote the potential of $WS_{\text{atm-CO2}}$ in the future need to be further explored.

The kinetics and driving mechanisms of carbonate dissolution have been analyzed in numerous studies[13,14]. The results have indicated that temperature and dissolved CO$_2$ in the water column are the two fundamental factors that determine the equilibrium state and the total CO$_2$ sequestration capacity of carbonate dissolution. In nature, carbonate rocks are dissolved mainly by soil water at the soil–rock interface. The amount of dissolved CO$_2$ in soil water is controlled largely by the soil partial CO$_2$ pressure (soil pCO$_2$)[15,16]. The pCO$_2$ level at the soil–rock interface is generally 3–10 times greater than that of the atmosphere, due to the abundant production of CO$_2$ by plant roots and soil biota[17]. Generally, an increasing soil pCO$_2$ level can greatly enhance the carbonate weathering intensity[18]. Therefore, variations in soil pCO$_2$ ultimately control [HCO$_3^-$] and its potential for atmospheric CO$_2$ capture in carbonate areas[18–20]. The role of temperature in controlling the carbonate weathering intensity ([HCO$_3^-$]) is also significant but complicated[15]. A higher temperature can enhance soil CO$_2$ production and the soil pCO$_2$ level, but it can also lower the solubility of CO$_2$ in the water column[3]. Thus, as the temperature increases, there may exist an optimal temperature range for carbonate dissolution due to the counterbalancing effect between thermodynamics (the impact of temperature on chemical reactions) and soil pCO$_2$[3,10,15]. Moreover, the dissolution and the equilibrium state of carbonate weathering can also be influenced by the solutions driven by non-carbonic acids (nitric or sulfuric acids), the weathering products of silicates, and water pH[21–24]. These factors can alter the activity coefficients and the major species of DIC in water systems, thereby changing the magnitude of carbonate-driven [HCO$_3^-$][3,13,14]. In addition, the changes in $WS_{\text{atm-CO2}}$ relevant to carbonate weathering are also controlled by water flow, which is also highly sensitive to global changes[25,26]. Therefore, these environmental factors are interlinked in controlling carbonate weathering, and such complex interrelations are the reason why it remains difficult to determine the fate of carbonate weathering in a changing global system[10].

Vegetation ecosystems capture large quantities of atmospheric CO$_2$, which plays a key role in regulating the global climate[27]. Vegetation cover is a crucial factor that dominates carbonate weathering on continental surfaces, and it is involved in most of the processes involving [HCO$_3^-$] production and $WS_{\text{atm-CO2}}$ generation[15,17]. The most significant control of vegetation cover on carbonate weathering intensity ([HCO$_3^-$]) is its impact on soil pCO$_2$[17–19]. A higher vegetation cover generally results in higher vegetation productivity and increased root-zone CO$_2$ production[19]. Variations in vegetation cover also change the soil moisture (SM), thereby influencing soil respiration and the air-fill space in the soil layer[16,28]. All these changes can impact soil pCO$_2$ and thus the carbonate weathering intensity. Although previous studies revealed that vegetation cover plays a key role in controlling [HCO$_3^-$], few studies have distinguished its individual influence on weathering from the mixed signals of other drivers (mostly temperature)[3,10,15]. Evidence from satellite images suggests that ~25–50% of the Earth's surface is undergoing greening (increase in vegetation greenness, 1982–2009) due to climate change and ecological restoration projects (ERPs), while

~4% exhibits browning[27]. The rapid increase in global vegetation greenness and the related carbon storage enhancement substantially neutralize anthropogenic CO$_2$ emissions[27,29]. Moreover, a growing number of studies have demonstrated that vegetation greenness and carbonate weathering intensity can increase synchronously[11,30,31]. In addition, it has been found that long-term vegetation restoration in carbonate areas can substantially enhance the concentrations of Ca^{2+} and HCO$_3^-$ in water and their export amount[7,12,30]. This implies that vegetation restoration has great potential for enhancing both vegetation ecosystem carbon storage (some of the organic carbon may be remineralized and returned to the atmosphere) and carbon capture by weathering. Given that vegetation coverage and temperature could be the most significant factors for [HCO$_3^-$] and $WS_{\text{atm-CO2}}$ in the future, the improved quantification of their individual impacts is important for understanding the fate of carbonate weathering and its role in the future global carbon cycle. Besides, a warming future is anticipated globally. Considering the negative impact of warming on the carbonate weathering intensity, it is important to determine whether a greening Earth can override the negative influence of warming on carbonate dissolution (reducing the carbonate solubility) and enhance the carbonate weathering intensity and its related weathering sink for atmospheric CO$_2$ at regional and global scales. This is critical information because it relates to whether this weathering sink for atmospheric CO$_2$ has the potential to be regulated by humans to mitigate future global warming. Therefore, systematic studies are urgently needed to determine the individual influence of greening on global carbonate weathering under a warming climate.

Carbonate rocks have an uneven global distribution and Southwest China is one of the most representative regions with extensive carbonate outcrops[32]. Over the past few decades, China has implemented several national-scale ERPs to alleviate ecological degradation in this region[33,34]. Climate change and the implementation of these ERPs over the past few decades have resulted in Southwest China becoming one of the greenest regions in the world[29,35]. Thus, the carbonate areas of Southwest China are well suited to evaluating the response of carbonate weathering to long-term changes in factors, such as vegetation greenness, temperature, and water flow, especially in temperate latitudes. Considering that vegetation greening can change soil pCO$_2$ by altering vegetation productivity, we applied a net primary productivity-based ecological model (NPP–pCO$_2$, see the Methods and Results sections for details) to simulate soil pCO$_2$ in regional and global carbonate areas. In addition, a chemical equilibrium model called the maximum potential dissolution (MPD) model was widely applied to calculate [HCO$_3^-$] in previous studies[3,5,36]. This model can separately estimate the individual impacts of thermodynamics and soil pCO$_2$ on [HCO$_3^-$] variations by fixing one of the parameters (temperature or pCO$_2$, see the Methods section for details). Hence, in this study, we utilized these biogeochemical models and a weathering-related atmospheric CO$_2$ sink equation to investigate the variations in [HCO$_3^-$] and $WS_{\text{atm-CO2}}$ in Southwest China. The influences of vegetation change and climatic warming on the long-term variations of [HCO$_3^-$], and the individual impacts of [HCO$_3^-$] and water flow changes on $WS_{\text{atm-CO2}}$ were estimated separately. The long-term trend of [HCO$_3^-$] production in global carbonate areas over the past few decades, and the impacts of warming and vegetation variations on carbonate weathering intensity, were also evaluated. To verify the findings of these models, we constructed an experimental test site in the field. This site has five artificial carbonate catchments which were built to study the changing patterns of carbonate weathering intensity ([HCO$_3^-$]) under different global change scenarios: the scenario controlled only by warming versus the scenario controlled by greening and warming. By using the long-term monitoring data (nearly 7 years) from this site, we can further verify and quantify the individual impacts from greening and warming on [HCO$_3^-$] (see the Methods section for details). We believe our findings contribute to an improved
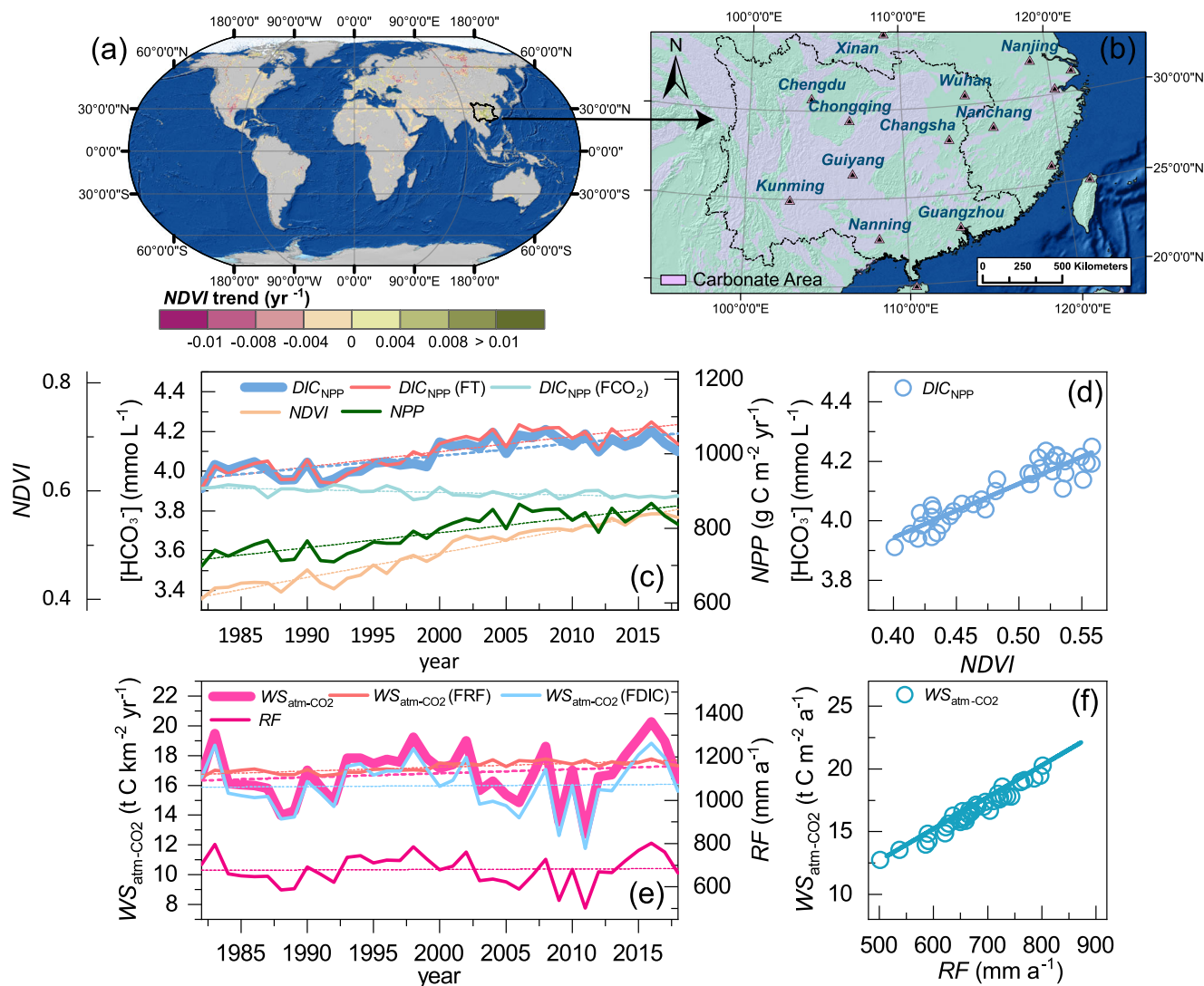
Fig. 1 | Long-term trends of vegetation greenness, carbonate weathering intensity ([HCO$_3^-$] as a proxy), and the Weathering Sink for atmospheric CO$_2$ (WS$_{atm-CO2}$) in the carbonate areas of Southwest China and global carbonate areas during the past ~4 decades. a Annual variations in mean normalized difference vegetation index (NDVI) in global carbonate areas during 1982–2018. **b** Location of the Southwest China carbonate areas. **c** Annual variations of normalized difference vegetation index (NDVI), net primary production (NPP, MUSES), and [HCO$_3^-$] in Southwest China. The curve of DIC$_{NPP}$ is [HCO$_3^-$] simulated using a net primary productivity-based soil pCO$_2$ model (NPP–pCO$_2$) and a carbonate equilibrium model (MPD). The curve of DIC$_{NPP}$ (FT) is [HCO$_3^-$] (DIC$_{NPP}$) with temperature fixed to the value in 1982, and DIC$_{NPP}$ (FCO$_2$) is [HCO$_3^-$] with pCO$_2$ also fixed to the value in 1982. **d** Relationship between simulated values of [HCO$_3^-$] (DIC$_{NPP}$) and NDVI. **e** Variations in WS$_{atm-CO2}$ and runoff depth (RF) in the carbonate areas of Southwest China during 1982–2018. The solid curve of WS$_{atm-CO2}$ represents the Weathering Sink for atmospheric CO$_2$ calculated by DIC$_{NPP}$ in **c** and RF. The curve of WS$_{atm-CO2}$ (FRF) is WS$_{atm-CO2}$ with RF fixed to the value in 1982, and WS$_{atm-CO2}$ (FDIC) is [HCO$_3^-$] fixed to the value in 1982. **f** Relationship between simulated WS$_{atm-CO2}$ values and RF. The dashed lines in the **c** and **e** are the long-term linear trends (linear fitting line) of different parameters.

understanding of the fate of chemical weathering related atmospheric CO$_2$ sink under global change, and the potential for utilizing geological carbon capture mechanism in mitigating ongoing global warming.

Results

Long-term environmental changes in Southwest China

We found that from 1982 to 2018, Southwest China experienced the largest increase (+0.0044 yr^{-1}) in annual mean normalized difference vegetation index (NDVI) (NDVI, as a proxy of vegetation greenness) among global carbonate areas (Fig. 1a). The net primary production (NPP) in this region also increased remarkably during this period (+4.0 g C m^{-2} yr^{-1}), showing a significant correlation with NDVI (Pearson's R = 0.93, with linear regression). To estimate the variations of carbonate weathering intensity in Southwest China and globally during this period, we first calculated the soil pCO$_2$ in carbonate areas using a NPP–pCO$_2$[10].

We then applied the simulated soil pCO$_2$ results, global temperature data, and a chemical equilibrium model (MPD) to calculate the spatio-temporal variations in [HCO$_3^-$] in carbonate areas (see the Methods section for details of the soil pCO$_2$ models and MPD). The results of simulated [HCO$_3^-$] (Fig. 1c, labeled as DIC$_{NPP}$) in Southwest China ranged from ~3.9 to ~4.2 (mmol L^{-1}), and the global average [HCO$_3^-$] calculated using the NPP–pCO$_2$ model was 3.2 (mmol L^{-1}). To verify the accuracy of these modeling results, we compared the simulated [HCO$_3^-$] values (DIC$_{NPP}$) with actual [HCO$_3^-$] measurements from the pure carbonate springs of 21 field sites on a global scale (Supplementary Table 1). We found that the simulated [HCO$_3^-$] values generally matched the actual [HCO$_3^-$] measurements at different globally-distributed field sites (Supplementary Fig. 1). In Southwest China, our simulated [HCO$_3^-$] results showed significant increasing trends with around +5.8% from 1982 to 2018 (Supplementary Fig. 2). As shown in Fig. 1d, the simulated [HCO$_3^-$]
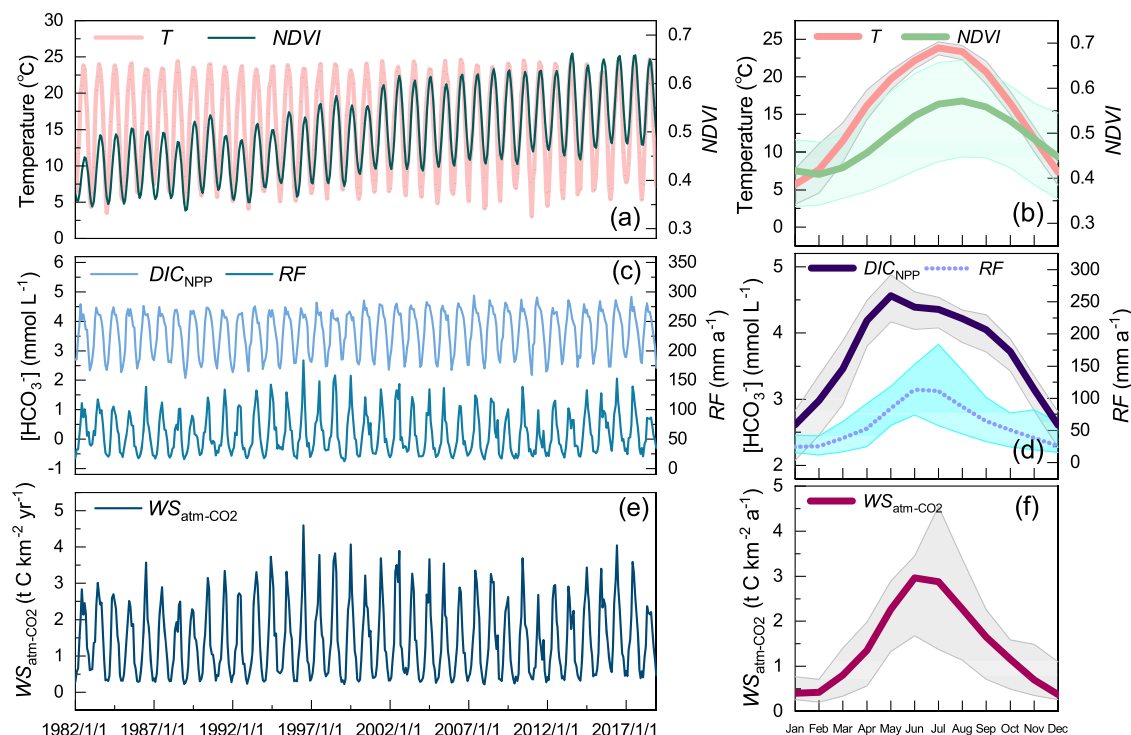
Fig. 2 | Seasonal trends and variations of different variables in the carbonate areas of Southwest China during 1982–2018. a Seasonal trends and **b** seasonal variations in temperature (*T*) and normalized difference vegetation index (*NDVI*). **c** Seasonal trends and **d** seasonal variations in [HCO$_3^-$] (*DIC*$_{NPP}$, simulated by a NPP–*p*CO$_2$ model and a carbonate equilibrium model (MPD)), and runoff depth (*RF*). **e** Seasonal trend and **f** seasonal variation in the Weathering Sink for atmospheric CO$_2$ (*WS*$_{atm-CO2}$). The shaded areas represent the standard deviations of different variables during the past nearly four decades.

had a significant positive relationship with NDVI (Pearson's *R* = 0.93, with linear regression). To distinguish the individual influences of temperature and soil *p*CO$_2$ on carbonate weathering variations, we calculated [HCO$_3^-$] (NPP–*p*CO$_2$ and MPD) by fixing the temperature and soil *p*CO$_2$ to the values in 1982. We found that warming with unchanged *p*CO$_2$ could reduce [HCO$_3^-$] in Southwest China by nearly −1.3% (Fig. 1c, *DIC*$_{NPP}$ (FCO$_2$)). In contrast, a nearly +7.4% increase in [HCO$_3^-$] was observed during the same period, excluding the impact of rising temperature (Fig. 1c, *DIC*$_{NPP}$ (FT)). To further validate the outcomes of models, we applied a Bayesian statistical model (PyMC3 package in a Python 3 environment, see the Methods section for details) and Chi-Square Test for Linear-by-Linear Association (SPSS 20) to test the sensitivity of different input parameters (*NPP* and temperature) to the [HCO$_3^-$] simulation, and to evaluate the significance of the NDVI, *NPP*, and [HCO$_3^-$] trends during the past nearly four decades. The results of the sensitivity test (Bayesian statistical model) indicated that nearly 77.92% of HCO$_3^-$ changes are attributed to the *NPP* (coefficient = 1.19, 100% probability of a positive NPP effect). The results of a Chi-Square Test (Linear-by-Linear Association) also indicated that the trends of *NDVI*, *NPP*, and [HCO$_3^-$] in Southwest China under different scenarios (*DIC*$_{NPP}$, *DIC*$_{NPP}$(FT), and *DIC*$_{NPP}$(FCO$_2$), Fig. 1c) were significant (*P* < 0.01), with a low uncertainty.

We further calculated the *WS*$_{atm-CO2}$ driven by carbonate weathering in Southwest China, and the results ranged from 12.7 to 20.3 t C km^{-2} yr^{-1}. The results of *WS*$_{atm-CO2}$ demonstrated increasing trends (+6.1%) during 1982–2018 (Fig. 1e and Supplementary Fig. 3). The variations of simulated *WS*$_{atm-CO2}$ were positively related to changes in runoff depth (*RF*) (Pearson's *R* = 0.93, with linear regression) (Fig. 1f). To distinguish the individual influences of runoff and [HCO$_3^-$] (*DIC*$_{NPP}$) on *WS*$_{atm-CO2}$ variations, we calculated *WS*$_{atm-CO2}$ by fixing the *RF* and [HCO$_3^-$] to the values in 1982. We found that an enhanced [HCO$_3^-$] with unchanged *RF* could raise the *WS*$_{atm-CO2}$ in Southwest China by nearly 7.3% (Fig. 1e, *WS*$_{atm-CO2}$ (FRF)). In contrast, there was no substantial increase in *WS*$_{atm-CO2}$ during the same period excluding the impact of

[HCO$_3^-$] variation (Fig. 1e, *WS*$_{atm-CO2}$ (FDIC)). The results of the sensitivity test (Bayesian statistical model) showed that nearly 79.49% of *WS*$_{atm-CO2}$ changes can be attributed to the *RF* (coefficient = 0.99, 100% probability of a positive *RF* effect). However, the results of the Bayesian statistical model and a Chi-Square Test (Linear-by-Linear Association) showed that the trends of *WS*$_{atm-CO2}$ and *WS*$_{atm-CO2}$ (FDIC) were not significant (*P* > 0.05). This is similar to the trend significance test result for *RF* (*P* > 0.05). By contrast, the trend of *WS*$_{atm-CO2}$ (FRF) was significant (*P* < 0.01, low uncertainty of trend). This indicates that the fluctuating *RF* signals (high uncertainty of trend) in Southwest China may obscure the large contribution of increasing [HCO$_3^-$] to *WS*$_{atm-CO2}$ enhancement. Thus, the trend of *WS*$_{atm-CO2}$ (FRF) can verify that *WS*$_{atm-CO2}$ has increased significantly from 1982 to 2018 (the trends of *WS*$_{atm-CO2}$ and *WS*$_{atm-CO2}$ (FRF) were similar, +6.1% vs +7.3%).

Seasonal variations and verification by a field experiment in Southwest China

We used a high-resolution meteorological database and remote sensing products to analyze the variations in seasonal temperature (*T*), NDVI, [HCO$_3^-$] (*DIC*$_{NPP}$), and *WS*$_{atm-CO2}$ in Southwest China from 1982 to 2018 (Fig. 2). The highest *NDVI*, [HCO$_3^-$], and *WS*$_{atm-CO2}$ values all occurred during the hot and humid summer, with much higher values than in winter. We summarized the long-term trends of [HCO$_3^-$] (*DIC*$_{NPP}$) in the four seasons (spring: March–May, summer: June–August, autumn: September–November, winter: December–February), and also simulated the [HCO$_3^-$] by fixing the temperature and soil *p*CO$_2$ (MPD and NPP–*p*CO$_2$) on the seasonal scale (Supplementary Fig. 4). The largest increase and decrease in [HCO$_3^-$] (+14.6% and −1.7%) both occurred in spring with fixed temperature and soil *p*CO$_2$. This seasonality in [HCO$_3^-$] is consistent with the findings of our studies in Southwest China[18,25,37], and it is also consistent with the field measurements at our local simulation test site (Fig. 3). At this site we constructed five artificial carbonate catchments (each 100 m^2), dominated by bare rock, bare soil, cropland,
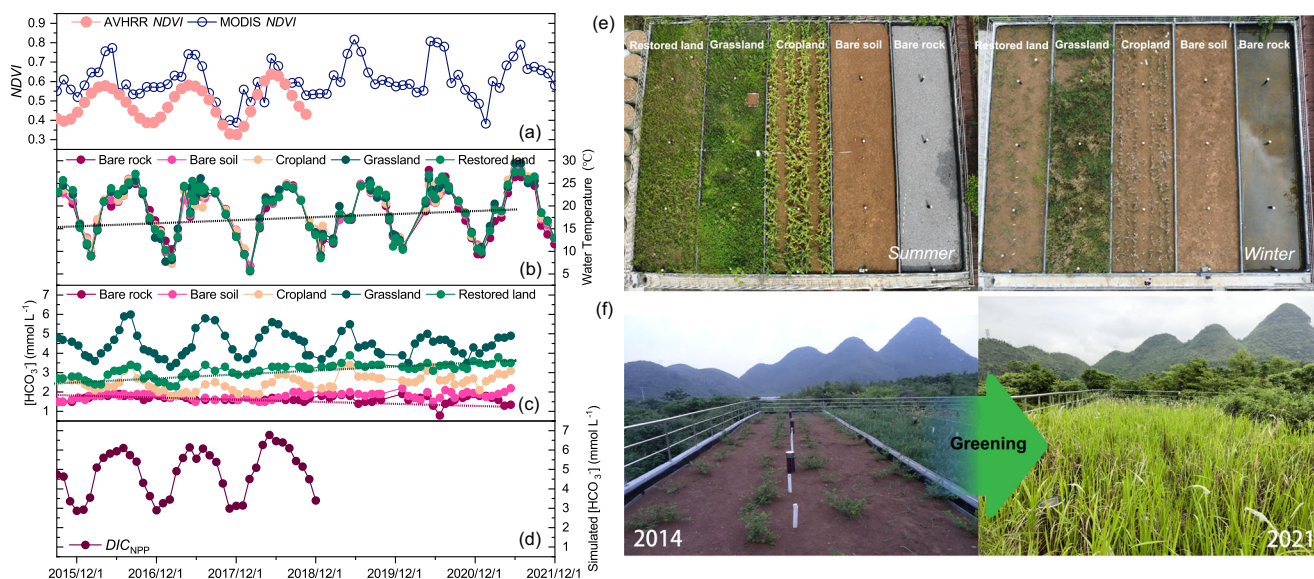
Fig. 3 | Seasonal changes in key parameters at the Puding Field Experimental Site in Southwest China from 2015 to 2021. a Normalized difference vegetation index (NDVI) (extracted from AVHRR and MODIS products), **b** water temperature (°C), **c** actual [HCO$_3^-$] measurements, and **d** simulated [HCO$_3^-$] (DIC_{NPP}). **e** five artificial carbonate catchments each with a different land-use type: bare rock, bare soil, cropland, grassland, and restored land (see the "Methods" section for details) **f** the vegetation change of restored land in the Puding field experimental site from 2015 to 2021. The dashed lines represent the overall trends (linear fitting line) of the different parameters.

grassland, and restored land, respectively[19]. Two of these carbonate catchments were constructed to study the [HCO$_3^-$] changing patterns under different global change scenarios. The bare rock-dominated catchment had no vegetation cover during 2015–2021, which simulates the scenario only controlled by warming. By contrast, we allowed the restored land-dominated catchment to transition from sparse shrubs to full vegetation coverage during the same period, which simulates the scenario controlled by greening and warming (see the Methods section for details). During nearly 7 years' (2015–2021) of continuous monitoring, we found that the simulated seasonal [HCO$_3^-$] (DIC_{NPP}) showed a similar seasonal pattern with the actual [HCO$_3^-$] of the grassland-dominated catchment of the test site (Fig. 3c, d). We also found that [HCO$_3^-$] in the restored land-dominated catchment had increased by +34.0% as the vegetation on the land surface rapidly changed from sparse shrubs to almost continuous grassland/shrubland in nearly 7 years (Fig. 3c, f and Supplementary Fig. 5). By contrast, [HCO$_3^-$] in the bare rock-dominated catchment at the test site decreased by −6.8% as the temperature increased during the same period. We also measured the seasonal water pH of these tanks from 2015 to 2017, and their pH ranged from 7.4 to 8.4 (Supplementary Fig. 6).

Variations on the global scale and in the future

To further distinguish the individual influences of warming and vegetation variations on [HCO$_3^-$] in various globally-distributed carbonate areas, we simulated the spatio-temporal variations of [HCO$_3^-$] (DIC_{NPP}) from 1982 to 2018, on the global scale. [HCO$_3^-$] estimated with a satellite-based vegetation index can be regarded as the actual weathering intensity, which exhibits an increasing trend (+2.4%) on the global scale for the past nearly four decades (<1% of uncertainty, 100% probability of positive *NPP* effect (coefficient = 0.96)). The largest increase in [HCO$_3^-$] was in the area between ~30°N and ~80°N, especially in Southwest China (Figs. 4a and 1c). Additionally, [HCO$_3^-$] decreased by −1.3% and increased by 3.7% from 1982 to 2018 (<1% uncertainty), with the temperature and soil pCO$_2$ held constant at the 1982 values, respectively. The simulated [HCO$_3^-$] at 30–80°N obtained by holding temperature and pCO$_2$ constant also demonstrated greater increases and decreases, respectively, than the actual values (Fig. 4b, c). We constructed an inverse modeling framework to calculate the

required NPP for the vegetation ecosystem to maintain an undiminished carbonate weathering intensity in the future (six CMIP6 models, RCP4.5, and RCP8.5). This resulted in NPP increases of 17.2–41.9%, 14.5–36.6%, and 3.6–16.7% for low, middle, and high latitudes, respectively (Fig. 5), which are the minimum values required to maintain a positive [HCO$_3^-$] trend in the future (2015–2100).

Discussion

Southwest China has experienced a remarkable greening trend over the past several decades[29,35,38]. The increase in vegetation greenness has increased the ecosystem carbon storage in this region[33]. In this study we also observed a simultaneous increase in NDVI and NPP in the carbonate areas of Southwest China during 1982–2018 (Fig. 1c). The simulated [HCO$_3^-$] shows an increasing trend and positive relationships with the variations in NDVI. This indicates that vegetation greening in the carbonate areas of Southwest China has resulted in a large enhancement in [HCO$_3^-$] over the past 37 years. To verify this increasing trend of [HCO$_3^-$] in Southwest China, we compared our simulation results with a case study in a typical carbonate catchment Houzhai in Southwest China[7]. Previous studies found that the forested area in this catchment experienced an 18.9% increase from 1986 to 2007. During the same period the groundwater [HCO$_3^-$] showed a remarkable increasing trend of 0.80 mg L^{-1} yr^{-1}. This value is consistent with the [HCO$_3^-$] trend (0.98 mg L^{-1} yr^{-1}) of DIC_{NPP} we estimated in this area (Supplementary Fig. 7). The results from our experimental test site also indicate that increased vegetation greenness can substantially increase [HCO$_3^-$] (Fig. 3). To further evaluate the control of vegetation on the carbonate weathering intensity on the global scale, we compiled the results of a series of global studies which conducted long-term monitoring of [HCO$_3^-$] and vegetation cover and compared them in detail with our simulated [HCO$_3^-$] trend. We found that our simulations (NPP–pCO$_2$) demonstrated a similar rising [HCO$_3^-$] trend to the results for the Konza Prairie in the USA (2.85 mg L^{-1} yr^{-1} vs 2.49 mg L^{-1} yr^{-1} (this study), ~15 years)[8] and the Ajoie region in Switzerland (1.72 mg L^{-1} yr^{-1} vs. 1.15 mg L^{-1} yr^{-1} (this study), ~22 years) during similar periods (Supplementary Fig. 7). Additionally, we analyzed [HCO$_3^-$] records from 21 globally-distributed pure carbonate springs with the land surface NDVI values at these spring sites and found a significant positive correlation (Supplementary Fig. 8).
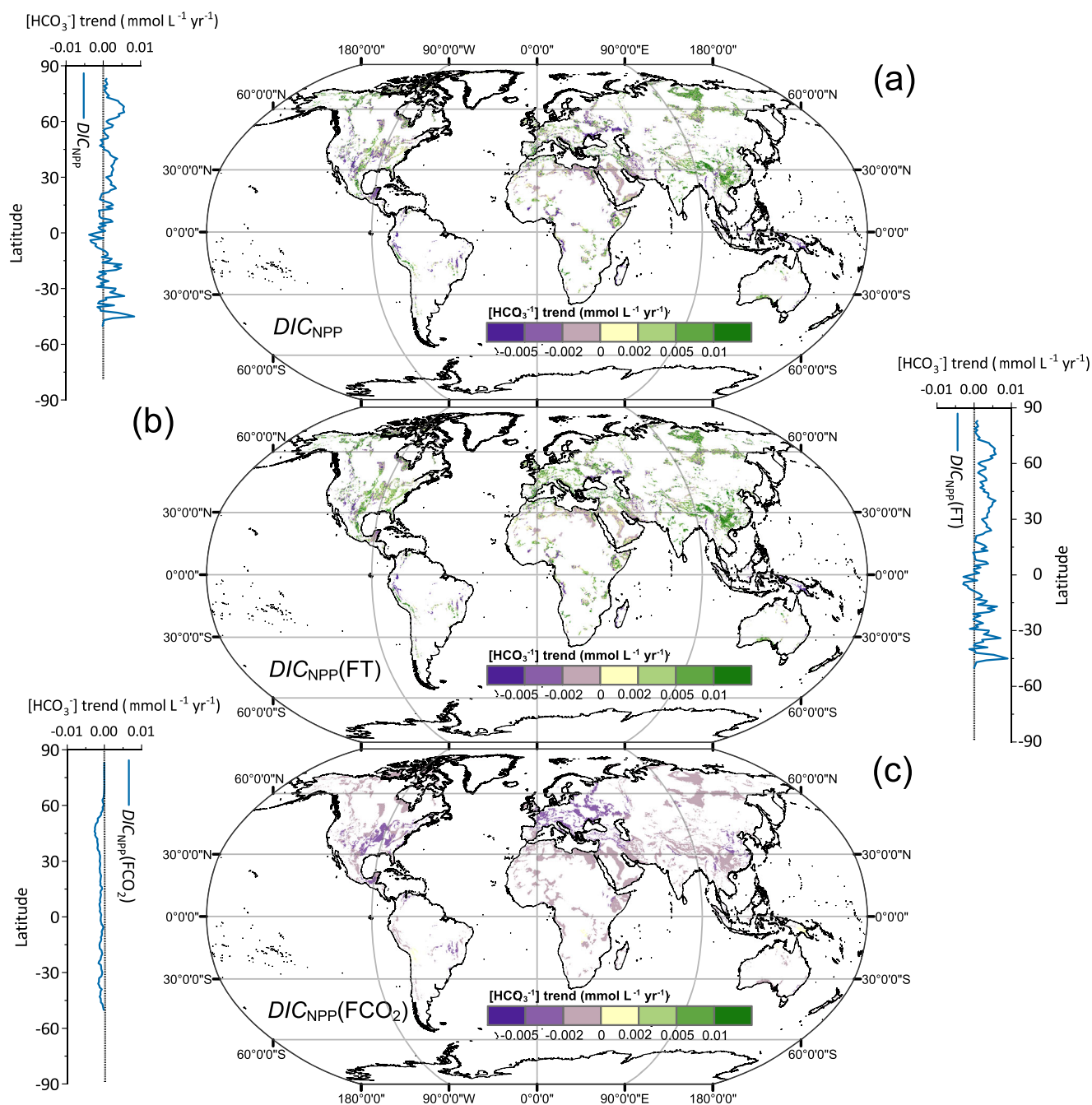
Fig. 4 | Spatio-temporal trends in carbonate weathering intensity [HCO₃⁻] in global carbonate areas from 1982 to 2018. a Spatio-temporal trends of [HCO₃⁻] (DIC_{NPP}) simulated by the NPP–pCO₂ model and a carbonate equilibrium model (MPD). **b** Spatio-temporal trends of simulated [HCO₃⁻] with temperature fixed to its 1982 value. **c** Spatio-temporal trends in [HCO₃⁻] with soil pCO₂ fixed to its 1982 value.

To sum up, this evidence, indicates that carbonate weathering responds sensitively to variations in vegetation cover on the global scale.

Previous studies of the influence of vegetation cover on carbonate weathering rarely considered the key function of vegetation in sustaining a high-dissolution rate under global change. Given the counterbalancing effects of thermodynamics and soil respiration on carbonate weathering[3,15], the "actual" increase in carbonate weathering related to vegetation greening is much greater than expected under a warming climate. If the influence of pCO₂ variations is ignored in carbonate weathering in the past nearly four decades, as shown in Fig. 1c, the individual impact of warming on carbonate dissolution in

Southwest China is undoubtedly negative (−1.3%). This indicates that the individual effect of vegetation cover on the increase in carbonate dissolution under the effect of thermodynamics should be around +7.1%. However, anthropogenic vegetation restoration can suppress the negative effect of the rising temperature in this region and force a significant increase in [HCO₃⁻] (Fig. 1c). These observations demonstrate the significant role of increased vegetation cover in maintaining the strong carbon capture capacity of carbonate weathering under a warming climate. This significant role is also evident in carbonate areas on the global scale. We found that global warming generally lowered the global [HCO₃⁻] with soil pCO₂ held constant (Fig. 4c). As the
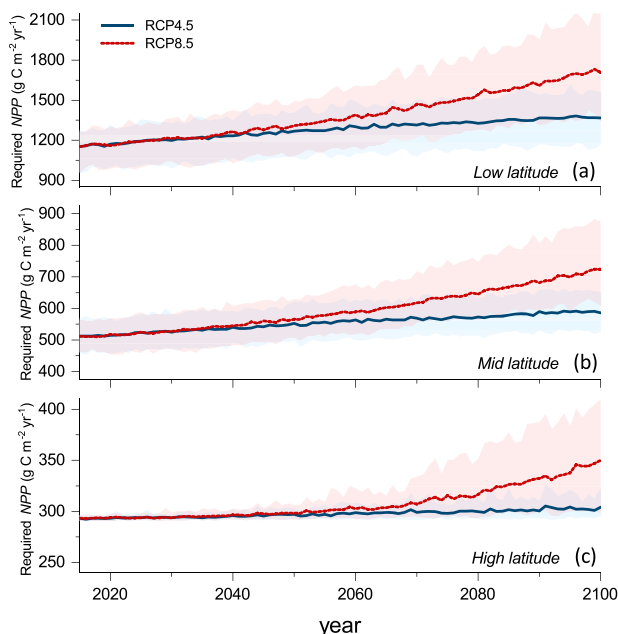
Fig. 5 | Required net primary production (NPP) for vegetation ecosystems to maintain an undiminished carbonate weathering intensity in the future (2015–2100). The shaded areas represent the standard deviations.

temperature was fixed (and not pCO_2) during the same period, [HCO_3^-] demonstrated a greater increase than the actual value. The results from our Puding field experimental site further confirmed the individual influence of vegetation cover on sustaining a high rate of carbonate weathering. Under the increasing temperature over the past ~7 years, [HCO_3^-] from the catchments with bare rock and vegetation restoration (restored land) show clear inverse trends (Supplementary Fig. 5), indicating that the development of a vegetation cover can reverse the negative carbonate weathering rate in a warming climate. Thus, these findings confirm our hypothesis that vegetation greening not only accelerates the carbonate dissolution rate but it also overrides the negative effect of warming on weathering intensity.

Flowing water is the main storage medium of the products of carbonate weathering. Due to the fast dissolution kinetics of carbonate, the total amount of carbonate weathering products of carbonate is statistically controlled by runoff variations[15,19,26], as shown in Fig. 2d. Water flow within a catchment is strongly influenced by the vegetation dynamics[39]. For instance, a higher vegetation cover can result in higher evapotranspiration (ET) for certain fragile ecosystems, thereby reducing the runoff[40]. Therefore, a paradox exists in that vegetation restoration can enhance [HCO_3^-] but reduce $WS_{atm\text{-}CO2}$. However, the long-term evidence from Southwest China indicates that carbonate areas may exhibit a different hydrologic response pattern compared to other ecosystems. Considering the remarkable increase in NDVI in the study area, the runoff coefficient (RC) (RF/Precipitation) should demonstrate large changes during 1982–2018, assuming that the vegetation cover exerts a major impact on the water flow and $WS_{atm\text{-}CO2}$. However, we found that the RC (RF/Precipitation, RC) in the carbonate areas and major catchments of Southwest China demonstrated only minor fluctuations or remained almost unchanged over the past 37 years (Supplementary Fig. 9). This indicates that vegetation restoration in humid carbonate areas can enhance the carbonate weathering intensity while sustaining a stable water yield[30]. We suggest that this can be attributed to the development of vertical pipes, sinkholes, and sub-surface conduit networks, facilitating the pathways of water flow to carbonate aquifers and groundwater[41]. Our results also demonstrate very large seasonal variations in [HCO_3^-] and $WS_{atm\text{-}CO2}$, and such seasonal differences were rarely considered in previous relevant studies. Considering that seasonal temperature,

vegetation cover, and water flux vary widely on a global scale, we suggest that in future research, high-resolution [HCO_3^-] and $WS_{atm\text{-}CO2}$ estimates are necessary. In summary, we stress that the vegetation increase in the carbonate areas of Southwest China may not cause a decrease in RF, while synchronous increases in [HCO_3^-] and $WS_{atm\text{-}CO2}$ can be expected under vegetation greening. These findings further suggest that a greening Earth can override the negative influence of warming on carbonate dissolution and enhance the carbonate weathering intensity and its relevant atmospheric CO_2 sink (Fig. 6).

After exploring the behavior of carbonate weathering under the linked effects of vegetation-temperature water in the contemporary dynamic Earth system, the central question arises—what is the maximum [HCO_3^-] enhancement that can ultimately by generated by vegetation restoration? The results of our simulation and test site evidence indicate that vegetation restoration in Southwest China can promote increases in [HCO_3^-] (by ~34.0%). However, what is the maximum potential of vegetation restoration on carbonate weathering enhancement at the global scale? To address this, we calculated the theoretical [HCO_3^-] in the global carbonate areas, assuming all the land cover is ultimately changing to forest, and then compared this value with the average global [HCO_3^-] during the past 37 years. Using the NCEAS model[42] for the forest NPP calculation, we found that vegetation restoration can result in a maximum increase of 43.8% in [HCO_3^-] (3.2 vs. 4.6 mmol L^{-1}) in the global carbonate areas. Considering that the $WS_{atm\text{-}CO2}$ will be further enhanced by an intensifying hydrological cycle due to the CO_2-induced warming and anthropogenic land-use changes[5,43], we suggest that future vegetation restoration is important not only for the carbon storage of ecosystems but also for enhancing maintaining the chemical weathering related atmospheric CO_2 sink.

Our results have revealed substantially increased carbonate weathering intensity and $WS_{atm\text{-}CO2}$ enhancements due to greening over the past decades in Southwest China. However, the results of our simulations at regional and global scales may have uncertainties derived from the effects of non-carbonic acids and the magnitude of silicate relative to carbonate dissolution. For instance, the increasing nitric and sulfuric acids from anthropogenic sources in the contemporary era have resulted in substantial carbonate mineral dissolution[22–24,44,45]. These dissolution processes have been identified as a carbon source rather than a carbon sink[21,46]. The neglect of their contributions could potentially cause an overestimation of atmospheric CO_2 drawdown by carbonate weathering[21]. The magnitude of [HCO_3^-] we simulated in the global carbonate areas can also be affected by the additional solute concentrations and a low water pH. A pure carbonate dissolution system is not always widely distributed in carbonate areas; and therefore, the silicate minerals in carbonate weathering-dominated areas can also supply solutes to the water column, although their impacts may be limited due to their lower solubility in systems with a short groundwater residence time. However, a long length of time for mineral–groundwater reaction can enhance the concentrations of these additional solutes, with significant impacts on activity coefficient values. This could affect the thermodynamic equilibrium modeling and result in uncertainties in [HCO_3^-] simulation. To estimate how non-carbonic acids and silicate mineral weathering affect equilibrium modeling, we used stream geochemical data from two carbonate-dominated catchments (the Garonne river and Beipan river), which are influenced, respectively, by nitric acid from the usage of N-fertilizer and sulfuric acid from the oxidation of sulfide minerals[22,47]. Using PHREEQC software, we estimated that the additions of non-carbonic acids and the products of the weathering of silicate minerals could lead to uncertainties of 2.6–6.4% for the equilibrium modeling of ([HCO_3^-]) for these two sites, respectively. In addition, the pH could be considerably lower in some natural water systems, given that the majority of the DIC may be converted to H_2CO_3, which also results in uncertainties in [HCO_3^-] simulation. In summary, the [HCO_3^-] and $WS_{atm\text{-}CO2}$ we simulated in this study assume a pure carbonate
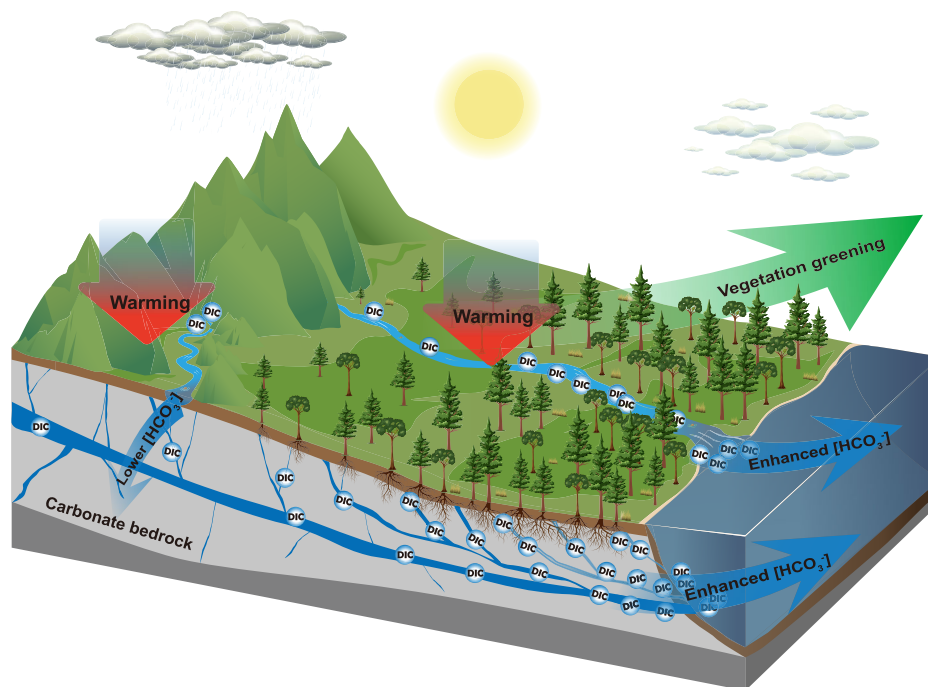
Fig. 6 | Cartoon illustrating the response of carbonate weathering under vegetation greening and a warming climate. The positive effect of a greening Earth on carbonate weathering overrides the negative influence of warming.

weathering system. Due to the complexity of the natural environment, several uncertainties need to be estimated globally in future research. Besides, to fully understand the fate of carbonate weathering in a greening Earth and the role of the related weathering sink for atmospheric CO_2 in the global carbon cycle, several issues should also be addressed. First, a stable water yield in humid Southwest China may not fully represent the hydrological features of several specific carbonate areas, especially in semi-arid and arid regions. Due to the major control of chemo-statistic behavior on continental weathering loads, an improved comparison of water yield responses to revegetation in different global carbonate regions is necessary for predicting the future $WS_{atm-CO2}$ at the global scale. Moreover, several studies have indicated that the loss of soil water is exacerbated in Southwest China due to the increase in the forested area[26]. These moisture losses may limit vegetation productivity and soil respiration and reduce the carbon capture potential for both ecosystems and weathering processes[16,48], which will need to be considered in the future. Additionally, long-term vegetation restoration can affect soil physical properties, such as soil temperature and soil porosity[28], which may alter the thermodynamics of carbonate dissolution and the CO_2 concentration in soil layers. The carbon weathering intensity and ecosystem functioning for some regions may be sensitive to these perturbations, which should be addressed in future research.
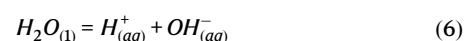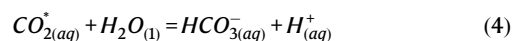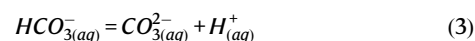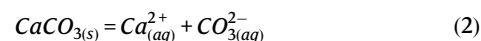
Methods
Carbonate weathering simulations
The research area in this study is located in Southwest China (102°25′–114°25′E, 21°59′–30°25′N), including eight provinces (Fig. 1). Southwest China is noted for its extensive carbonate outcrops (total of ~9.7 × 10⁵ km², mainly limestone) and diverse karst landscapes[32]. This area is dominated by a subtropical monsoon climate and rainfall events are concentrated from April to September[49]. In the last century, deforestation, and damaging cultivation practices caused widespread rock desertification and ecosystem degradation in the carbonate areas of Southwest China[50]. Hence, China has invested nearly 19 billion USD to implement several national ERPs in this region since the 1980s[34]. These ERPs have resulted in a substantial increase in vegetation cover

and have led to Southwest China becoming one of the most striking greening regions worldwide over the past few decades[33,35] (Fig. 1a, b). In this study, we focused on the carbonate areas in Southwest China and simulated the variations in $[HCO_3^-]$ and $WS_{atm-CO2}$ during this greening period. Additionally, we simulated $[HCO_3^-]$ in the global carbonate areas during the same period. Details of the biogeochemical models (NPP–pCO_2 and MPD), calculations, and the multi-source database used in the simulations are given below.

Carbonate weathering intensity estimation. In previous studies, we applied an MPD to calculate the equilibrium concentration of $[HCO_3^-]$ as a function of temperature and soil pCO_2[10]. In this study we used the results of this carbonate equilibrium model (simulated $[HCO_3^-]$) to represent the actual $[HCO_3^-]$ at the global scale. This model can also separately estimate the individual influences from thermodynamics (temperature) and soil pCO_2 variations. Equation 1 is a simplified equation to represent how carbonate weathering captures atmospheric CO_2. Actually, for a pure calcite dissolution system, the weathering of carbonate is controlled by a series of chemical equations[2,3,13]:

$$CaCO_{3(s)} = Ca^{2+}_{(aq)} + CO^{2-}_{3(aq)} \tag{2}$$

$$HCO^-_{3(aq)} = CO^{2-}_{3(aq)} + H^+_{(aq)} \tag{3}$$

$$CO^*_{2(aq)} + H_2O_{(1)} = HCO^-_{3(aq)} + H^+_{(aq)} \tag{4}$$

$$CO^*_{2(g)} = CO^*_{2(aq)} \tag{5}$$

$$H_2O_{(1)} = H^+_{(aq)} + OH^-_{(aq)} \tag{6}$$

These equations are governed by different mass action laws, which are controlled by the temperature-dependent reaction constants K_1, K_C, K_H, and K_2, and the temperature, T (°C)[13]. K_1 and K_2 are the first and second dissociation constants for carbonic acid in water (Eq. 4

and Eq. 3), and K_c is the equilibrium constant for calcite dissolution (Eq. 2). K_H is the Henry's Law constant for CO_2 gas in water (Eq. 5)[14]. These reactions are characterized by rapid kinetics and the drainage water can reach an equilibrium state within a couple of hours[13]. The pCO_2 (atm) at the water–rock interface (atmosphere or soil) is an additional determinant of the magnitude of HCO_3^- production[13].

In nature, the water interacting with $CaCO_3$ is impure and the activity coefficient should be introduced to relate concentrations to activities. We can denote γ_1 and γ_2 as the activity coefficients for single-charged and double-charged species, respectively, and the Davies equation can then be applied to calculate the activity coefficients[3]:

$$\log(\gamma) = -Az^2 \left(\frac{\sqrt{I}}{1+\sqrt{I}} - 0.3\sqrt{I} \right) \tag{7}$$

Here, A is a constant based on temperature, z is the charge of the chemical species, and I is the ionic strength of the solution. Assuming that in a natural water body (pH ~8), the solutes include several common single-charged and double-charged species (Ca^{2+}, Mg^{2+}, Na^+, K^+, HCO_3^-, CO_3^{2-}, SO_4^{2-}, NO_3^-, and Cl^-), then the electro-neutrality of its composition implies that:

$$2[Ca^{2+}] + 2[Mg^{2+}] + [Na^+] + [K^+] + [H^+] \\ = 2[CO_3^-] + 2[SO_4^{2-}] + [HCO_3^-] + [NO_3^-] + [Cl^-] + [OH^-] \tag{8}$$

We can then group the species with no acid-base behavior and neglect H^+, OH^- and CO_3^{2-}, and Eq. 7 can be modified to:

$$2[Ca^{2+}] = [HCO_3^-] + RA \tag{9}$$

with $RA = 2[SO_4^{2-}] + [NO_3^-] + [Cl^-] - 2[Mg^{2+}] - [Na^+] - [K^+]$ being the reduced alkalinity[3]. In this study, we mainly consider the influences of greening and warming on soil pCO_2 and the thermodynamics (temperature-dependent reaction constants). Thus, an ideal pure calcite dissolution–controlled system is assumed in global carbonate areas. Under such conditions RA can set to 0 at equilibrium (the solutions only contain the ionic species Ca^{2+}, HCO_3^-, CO_3^{2-}, H^+, and OH^-), and then the equilibrium HCO_3^- concentration ($[HCO_3^-]_{eq}$) can be calculated by refs. 3,13,36:

$$[HCO_3^-]_{eq} = \left(\frac{2K_1(T)K_C(T)K_H(T)}{K_2(T)\gamma_{Ca^{2+}}\gamma_{HCO_3^-}^2} pCO_2 \right)^{1/3} \tag{10}$$

Here, all the K constants can be estimated by temperature. pCO_2 (atm) is the partial pressure of CO_2 at the water–rock interface, which can be estimated by soil pCO_2 models. γCa^{2+} and γHCO_3^- are the activity coefficients for Ca^{2+} and HCO_3^- at equilibrium (Ca^{2+} and HCO_3^- are assumed to be the only single-charged and double-charged species in the pure calcite dissolution system), which can be calculated using Eq. 6. T is the temperature in °C. To save computing time for long-term and large-scale spatial evaluations, we applied an approximate equation which summarizes all the equations (Eqs. 2–8) for ideal calcite dissolution at equilibrium:

$$[HCO_3^-]_{eq} \approx 20.75 \cdot (1 - 0.0139T) \sqrt[3]{pCO_2} \tag{11}$$

This equation requires only temperature and pCO_2 and is valid for $pCO_2 > 3 \times 10^{-4}$ [51].

Soil pCO_2 parameterizations. Soil pCO_2 is a critical parameter for $[HCO_3^-]$ simulation. In previous studies, soil pCO_2 was estimated by different ecological models based on empirical relationships and processes. T, ET, NPP, and SM are the common environmental parameters applied in these models for soil pCO_2 simulation. These parameters are also controlled by vegetation cover variations. In this study, we selected a net primary productivity-based soil pCO_2 models for estimating long-term carbonate weathering intensity. This model can generate accurate simulations across different land-use types at a global scale. Details of these pCO_2 models are given below[3]:

NPP–based soil pCO_2 (NPP–pCO_2) is a semi-mechanistic model which calculates the pCO_2 profile across soil layers. In this model, CO_2 production in the root zone is assumed to be 75% of NPP[52]. This ratio is based on a large-scale statistical analysis of in-situ aboveground and belowground carbon measurements for 79 global sites[53]. Soil pCO_2 can then be expressed as a function of the atmospheric CO_2 concentration, temperature, and the NPP of the vegetation ecosystem[3]:

$$pCO_{2(soil)} = pCO_{2(atm)} + \frac{A \cdot 0.75 \cdot NPP}{T^2} \tag{12}$$

where A is the set of conversion unit constants. In this study, the A values for annual and seasonal pCO_2 were set to 1.03×10^6 and 1.236×10^7, pCO_{2atm} is the atmospheric CO_2 pressure (ppmv) NPP in grams of dry matter per m^2 for a given year or month (g m^{-2} yr^{-1}/month^{-1}), T is the temperature (K), and $pCO_{2(soil)}$ is the maximum CO_2 pressure reached beneath the root zone (at the soil–rock interface) (ppmv). In previous studies, we compared the results of the NPP–pCO_2 model with field measurements from different global individual studies[5,10]. We found that the model produced very accurate results and was widely applicable in different land cover types. Hence, we used NPP–pCO_2 to simulate seasonal $[HCO_3^-]$ variations in Southwest China and for global carbonate areas. Additionally, to evaluate the influences of vegetation production and warming on future global $[HCO_3^-]$, we constructed an inverse modelling framework based on NPP–pCO_2 and NCEAS model (NPP = $2540/(1+\exp(1.584-0.0622\,T))$)[36]. We applied the future temperature data from six CMIP6 models to estimate the required NPP, which can sustain an undiminished global carbonate weathering intensity.

Weathering related atmospheric CO_2 sink calculation. To calculate the total atmospheric CO_2 capture produced by minerals weathering, we used a weathering-related atmospheric CO_2 sink equation ($WS_{atm-CO2}$) [t C km^{-2} yr^{-1}][2]:

$$WS_{atm-CO2} = 10^{-3} \cdot (nf_c + nf_s) \cdot [HCO_3^-] \cdot m_r \cdot RF \tag{13}$$

Here, $WS_{atm-CO2}$ (t C km^{-2} yr^{-1}) is the weathering sink for atmospheric CO_2. RF (mm) is the RF, $[HCO_3^-]$ (mmol L^{-1}) is the bicarbonate concentration (simulated by an NPP–pCO_2 and MPD) driven by carbonates and silicates weathering, and m_r (g mol^{-1}) is the molar mass of carbon. f_c and f_s are the fractions of HCO_3^- produced by carbonate and silicate weathering, respectively. The partitioning factor n is 1 for silicate weathering, and 0.5 for carbonate weathering, as in the latter case one part of $[HCO_3^-]$ is from atmospheric CO_2 and the other part is from carbonate rock. In this study, we only calculate the $WS_{atm-CO2}$ driven by carbonate weathering.

Model sensitivity testing and trend uncertainty evaluation. The sensitivity testing of input parameters to models and the trend uncertainty evaluation are significant to validate the model simulation results. In this study, we applied a Bayesian statistical model[54] by using the PyMC3 package (version 3.10) in a Python 3 environment to evaluate the sensitivity of input parameters on $[HCO_3^-]$ and $WS_{atm-CO2}$ simulations. PyMC3 is an open-source probabilistic programming framework with an intuitive and readable, yet powerful, syntax that is close to the natural syntax statisticians use to describe models. It features next-generation Markov chain Monte Carlo sampling algorithms. We used PyMC3 to construct a Bayesian multivariate linear regression and posterior analysis by using modeling $[HCO_3^-]$ results (or $WS_{atm-CO2}$) and its drivers (model input parameters). Then, the
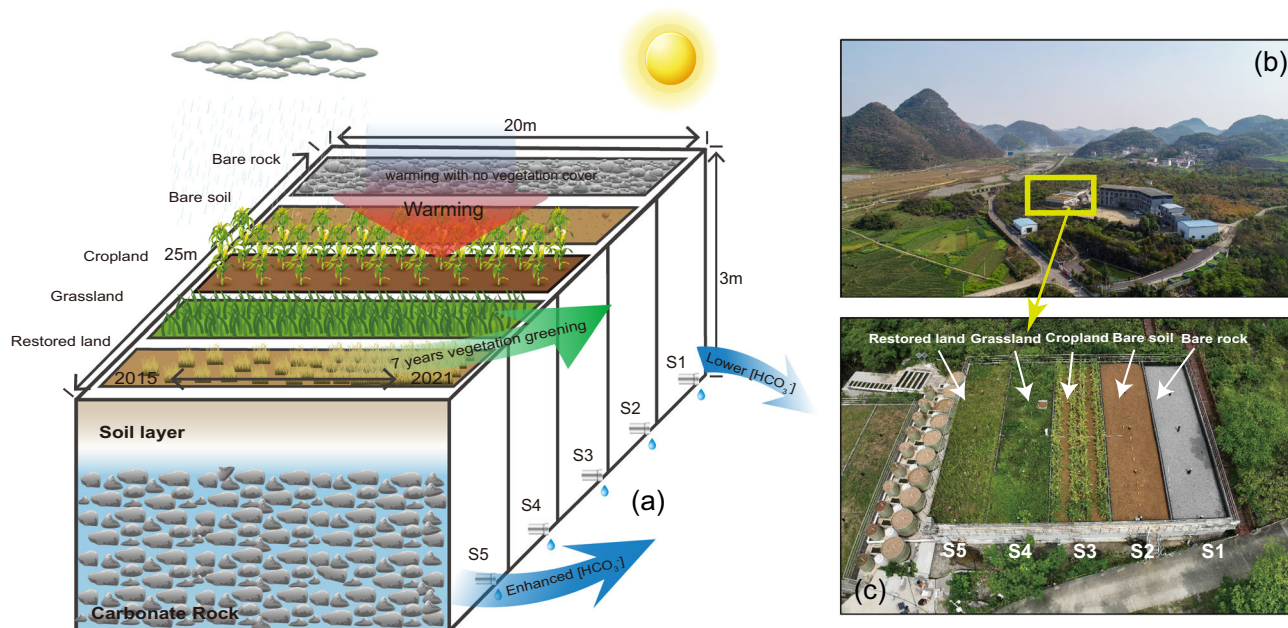
Fig. 7 | The structure and the carbonate weathering simulations of the Puding experimental test site. a Five constructed artificial carbonate catchments (each 100 m²) dominated by bare rock (S1), bare soil (S2), cropland (S3), grassland (S4), and restored land (S5). The groundwater $[HCO_3^-]$ was continuously measured from 2015 to 2021. The bare rock-dominated catchment (S1) had no vegetation cover during 2015–2021, which simulates the scenario of carbonate weathering controlled only by warming. The restored land–dominated catchment (S5) experienced nearly 7 years' vegetation restoration during 2015–2021, which simulates the scenario of carbonate weathering controlled by greening and warming. **b** and **c** are drone photos for the Puding Comprehensive Karst Research and Experimental Station and experimental test site, respectively.

sensitivity of input parameters to the model outcomes (their contributions and significances) was quantified. In addition, to further evaluate the significance of long-term trends in simulated $[HCO_3^-]$ (or $WS_{atm-CO2}$) and its drivers, we also conducted trend uncertainty tests using Chi-Square Test for Linear-by-Linear Association (SPSS 20 software, Crosstabs). The P value of this test is applied to validate the credibility of the trends of $[HCO_3^-]$ (or $WS_{atm-CO2}$) ($P < 0.01$ presents a significant trend with low uncertainty).

Materials. To estimate the long-term weathering intensity in the global carbonate areas, we utilized digital global carbonate area boundary data and different high-resolution databases (meteorological parameters, vegetation index, runoff, and NPP from 1982 to 2018). The world karst aquifer map (WOKAM) produced by the Product Center of the Federal Institute for Geosciences and Natural Resources was used to extract the simulated $[HCO_3^-]$ values in the global carbonate areas. Due to uncertainties in precisely distinguishing limestone from the globally less common dolostone on the geological map, we calculated the carbonate weathering intensity by assuming that all carbonates are mainly calcite. The carbonate areas in WOKAM are divided into "continuous" and "discontinuous" amounts of carbonate minerals mixed with silicate minerals. Due to the very fast kinetics of carbonate weathering compared to silicates[55,56], we assumed that the weathering processes in these carbonate terrains are dominated by a pure calcite dissolution system. The NOAA CDR AVHRR NDVI V5 (5 km) was used to evaluate the spatio-temporal greening trend within the carbonate areas during 1982–2018. The original grid data were aggregated to monthly NDVI using the maximum value composite method in the Google Earth engine and then summarized to annual mean *NDVI*. To more accurately represent the NDVI changes around our experimental site (Puding), we extracted high-resolution MODIS monthly NDVI data near the Puding Comprehensive Karst Research and Experimental Station using MOD13A1 products. The runoff data in the carbonate areas of Southwest China were from the China Natural Runoff Dataset version 1.0, with a spatial resolution of 0.25° × 0.25° (CNRD v1.0, tpdc.

ac.cn). The runoff data of major river catchments in Southwest China were obtained from national hydrological stations at the outlet of each catchment. NPP was the key input parameter for the three soil pCO_2 models used in this study. We obtained 8-day NPP data from the MUSES NPP database (MUltiscale Satellite remote Sensing products, https://muses.bnu.edu.cn/). The 8-day NPP data from MUSES were recalculated to monthly NPP values. The temperature used for $[HCO_3^-]$ calculations and the precipitation for RC estimations were from the CRUTEM 5.0 database (https://crudata.uea.ac.uk), with a spatial resolution of 0.5° × 0.5°. To estimate the $RNPP$ for sustaining stable future $[HCO_3^-]$, we used the future near-surface air temperature of two scenarios (2015–2100, SSP126-Sustainable and SSP585-Development paths based on fossil fuels) from six CMIP6 models (ACCESS-ESM1-5, BCC-CS M2-MR, CanESM5, CNRM-CM6-1, IPSL-CM6A-LR, and MPI-ESM1–2-LR) outcomes from the DKRZ archive https://esgf-data.dkrz.de/projects/cmip6-dkrz/. To optimize the calculation time, all the above-mentioned spatial data were re-projected onto a grid with a resolution of 0.25° × 0.25°.

Field experiment
To verify and quantify the individual influences from vegetation cover change and warming on carbonate weathering, we constructed a simulation test site (Puding Site) in the central area of Southwest China. This site is located in the Puding Comprehensive Karst Research and Experimental Station, Puding County, Guizhou Province, Southwest China (Figs. 3e and 7). This area experiences a humid sub-tropical monsoon climate with an annual mean air temperature of 15.1°C; and the mean annual precipitation is 1315 mm, 80% of which falls in the wet season from May to September. In January 2014, five concrete tanks with water pipe outlets, S1–S5, were built at the Puding experimental station, each simulating a carbonate catchment with a groundwater outlet under a single land-use scenario (Fig. 7a).

Each tank is 20-m long, 5-m wide, and 3-m deep, coated with epoxy resin (to avoid the influence of possible concrete erosion on tank hydrochemistry), filled with 2 m of dolomitic limestone rubble in the

lower part, and topped with 0.5 m of soil. One water pipe was set at the bottom of each tank, which can be regarded as a groundwater outlet. Tank S1 was left with bare carbonate rocks, to provide a scenario without soil and plants. Tank S2 simulates land with bare soil and underlying carbonate rubble. Tank S3 was planted with corn to simulate intensive cultivation. Alfalfa was sown in the soil of Tank S4 to simulate grassland land use. The soil of tank S5 was first sown with a small proportion of *Rosa roxburghii* (a native shrub species in this area) in 2014 (Fig. 7a). To simulate land with vegetation restoration, we then allowed the natural growth of grasses and shrubs. During 2014–2021 the surface of S5 was fully covered by natural vegetation (Fig. 3f). A lateral drainage hole in each tank simulated a natural carbonate spring. Each tank system thus simulated a single land-use catchment with precisely known, identical dimensions, and with the same climatic and geological conditions[37,57]. The water flow of each simulated catchment was controlled and the water temperature and $[HCO_3^-]$ concentration were measured monthly from 2015 to 2021. Thus, the bare rock-dominated catchment (S1) had no vegetation cover during 2015–2021, which simulates the scenario of carbonate weathering only controlled by warming. By contrast, the restored land-dominated catchment (S5) changed from a sparse shrub cover to full vegetation cover during the same period, which simulates the scenario of carbonate weathering controlled by greening and warming. The individual influences of greening and warming on $[HCO_3^-]$ could thus be further verified and quantified for this site.

Data availability

Source data are provided with this paper. The data are published openly in Figshare at https://doi.org/10.6084/m9.figshare.26232266. They include the data for plotting figures; vector boundary data of carbonate areas and river catchments; location data of 21 global carbonate springs; and input data with corresponding results for models and sensitivity analysis.

Code availability

All the codes for the models are published and freely available in Figshare at https://doi.org/10.6084/m9.figshare.26232266. They include the codes and input data for the following models: NPP–pCO₂, NCEAS, MPD; the Bayesian statistical model for sensitivity and uncertainty testing; and the $WS_{\text{atm-CO2}}$ calculation.

References

1. Berner, R. A. Weathering, plants, and the long-term carbon cycle. *Geochim. Cosmochim. Acta* **56**, 3225–3231 (1992).
2. Liu, Z., Dreybrodt, W. & Wang, H. A new direction in effective accounting for the atmospheric CO2 budget: considering the combined action of carbonate dissolution, the global water cycle and photosynthetic uptake of DIC by aquatic organisms. *Earth-Sci. Rev.* **99**, 162–172 (2010).
3. Gaillardet, J., Calmels, D., Romero-Mujalli, G., Zakharova, E. & Hartmann, J. Global climate control on carbonate weathering intensity. *Chem. Geol.* **527**, 118762 (2019).
4. Beaulieu, E. High sensitivity of the continental-weathering carbon dioxide sink to future climate change. *Nat. Clim. Chang.* **2**, 346–349 (2012).
5. Zeng, S., Liu, Z. & Kaufmann, G. Sensitivity of the global carbonate weathering carbon-sink flux to climate and land-use changes. *Nat. Commun.* **10**, 5749 (2019).
6. Raymond, P. A., Oh, N.-H., Turner, R. E. & Broussard, W. Anthropogenically enhanced fluxes of water and carbon from the Mississippi River. **451**, 449–452 (2008).
7. Yan, J., Li, J., Ye, Q. & Li, K. Concentrations and exports of solutes from surface runoff in Houzhai Karst Basin, southwest China. *Chem. Geol.* **304–305**, 1–9 (2012).
8. Macpherson, G. L. et al. Increasing shallow groundwater CO₂ and limestone weathering, Konza Prairie, USA. *Geochim. Cosmochim. Acta* **72**, 5581–5599 (2008).
9. Drake, T. W. et al. Increasing alkalinity export from large Russian Arctic rivers. *Environ. Sci. Technol.* **52**, 8302–8308 (2018).
10. Zeng, S., Kaufmann, G. & Liu, Z. Natural and anthropogenic driving forces of carbonate weathering and the related carbon sink flux: a model comparison study at global scale. *Glob. Biogeochem. Cycles* **36**, e2021GB007096 (2022).
11. Ulloa-Cedamanos, F. et al. Potential influence of landscape transition on stream water chemistry trends during the last decades in a karst catchment (Pyrenees, SW France) in a context of global environmental changes. *Ecol. Indic.* **140**, 109023 (2022).
12. Xiao, W. et al. Different responses of ecohydrological processes in the re-vegetation area between the dip and anti-dip slope in a karst rocky desertification area in southwestern China. *Plant Soil* **475**, 25–43 (2022).
13. Dreybrodt, W. Kinetics of the dissolution of calcite and its applications to karstification. *Chem. Geol.* **31**, 245–269 (1980).
14. Buhmann, D. & Dreybrodt, W. The kinetics of calcite dissolution and precipitation in geologically relevant situations of karst areas. *Chem. Geol.* **48**, 189–211 (1985).
15. Zeng, S. et al. Comparisons on the effects of temperature, runoff, and land-cover on carbonate weathering in different karst catchments: insights into the future global carbon cycle. *Hydrogeol. J.* **29**, 331–345 (2021).
16. Romero-Mujalli, G., Hartmann, J., Börker, J., Gaillardet, J. & Calmels, D. Ecosystem controlled soil-rock pCO2 and carbonate weathering—constraints by temperature and soil water content. *Chem. Geol.* **527**, 118634 (2019).
17. Berner, R. A. The rise of plants and their effect on weathering and atmospheric CO₂. *Sci. New Ser.* **276**, 544–546 (1997).
18. Liu, Z., Li, Q., Sun, H. & Wang, J. Seasonal, diurnal and storm-scale hydrochemical variations of typical epikarst springs in subtropical karst areas of SW China: Soil CO2 and dilution effects. *J. Hydrol.* **337**, 207–223 (2007).
19. Zeng, Q. et al. Carbonate weathering-related carbon sink fluxes under different land uses: a case study from the Shawan simulation test site, Puding, Southwest China. *Chem. Geol.* **474**, 58–71 (2017).
20. Raich, J. W. & Tufekcioglu, A. Vegetation and soil respiration: correlations and controls. *Biogeochemistry* **48**, 71–90 (2000).
21. Martin, J. B. Carbonate minerals in the global carbon cycle. *Chem. Geol.* **449**, 58–72 (2017).
22. Perrin, A.-S., Probst, A. & Probst, J.-L. Impact of nitrogenous fertilizers on carbonate dissolution in small agricultural catchments: Implications for weathering CO2 uptake at regional and global scales. *Geochim. Cosmochim. Acta* **72**, 3105–3123 (2008).
23. Torres, M. A., West, A. J. & Li, G. Sulphide oxidation and carbonate dissolution as a source of CO2 over geological timescales. *Nature* **507**, 346–349 (2014).
24. Oberhelman, A., Martin, J. B. & Flint, M. K. Sources of limestone dissolution from surface water-groundwater interaction in the carbonate critical zone. *Chem. Geol.* **662**, 122229 (2024).
25. Zeng, C., Liu, Z., Zhao, M. & Yang, R. Hydrologically-driven variations in the karst-related carbon sink fluxes: Insights from high-resolution monitoring of three karst catchments in Southwest China. *J. Hydrol.* **533**, 74–90 (2016).
26. Zhong, J., Li, S., Ibarra, D. E., Ding, H. & Liu, C. Solute production and transport processes in Chinese monsoonal rivers: implications for global climate change. *Glob. Biogeochem. Cycles* **34**, e2020GB006541 (2020).
27. Zhu, Z. et al. Greening of the Earth and its drivers. *Nat. Clim. Change* **6**, 791–795 (2016).

28. Goddéris, Y., Williams, J. Z., Schott, J., Pollard, D. & Brantley, S. L. Time evolution of the mineralogical composition of Mississippi valley loess over the last 10kyr: climate and geochemical modeling. *Geochim. Cosmochim. Acta* **74**, 6357–6374 (2010).

29. Chen, C. et al. China and India lead in greening of the world through land-use management. *Nat. Sustain.* **2**, 122–129 (2019).

30. Yan, J., Wang, W., Zhou, C., Li, K. & Wang, S. Responses of water yield and dissolved inorganic carbon export to forest recovery in the Houzhai karst basin, Southwest China: response of water yield and carbon export to forest recovery. *Hydrol. Process.* **28**, 2082–2090 (2014).

31. Yanes, J. L. & Moral, F. Spatial variability of hydrochemistry and environmental controls in karst aquifers of the Southern Iberian peninsula: implications for climate change impact assessment. *Sci. Total Environ.* **907**, 168141 (2024).

32. Goldscheider, N. et al. Global distribution of carbonate rocks and karst water resources. *Hydrogeol. J.* **28**, 1661–1677 (2020).

33. Tong, X. et al. Increased vegetation growth and carbon stock in China karst via ecological engineering. *Nat. Sustain.* **1**, 44–50 (2018).

34. Yi, R., Xu, X., Zhang, Y., Ye, Z. & Wang, K. Grain for green project may not threaten ecosystem sustainability by degrading water availability in humid karst landscapes. *Water Resour. Res.* **59**, e2022WR032415 (2023).

35. Brandt, M. et al. Satellite-observed major greening and biomass increase in South China karst during recent decade. *Earths Future* **6**, 1017–1028 (2018).

36. Gombert, P. Role of karstic dissolution in global carbon cycle. *Glob. Planet. Change* **33**, 177–184 (2002).

37. Zeng, Q. Carbonate weathering-related carbon sink fluxes under different land uses—a case study from the Shawan Simulation test site, Puding, Southwest China. *Chem. Geol.* **474**, 58–71 (2017).

38. Zhang, J., Liesch, T., Chen, Z. & Goldscheider, N. Global analysis of land-use changes in karst areas and the implications for water resources. *Hydrogeol. J.* **31**, 1197–1208 (2023).

39. Zhang, L., Dawes, W. R. & Walker, G. R. Response of mean annual evapotranspiration to vegetation changes at catchment scale. *Water Resour. Res.* **37**, 701–708 (2001).

40. Hoek Van Dijke, A. J. et al. Shifts in regional water availability due to global tree restoration. *Nat. Geosci.* **15**, 363–368 (2022).

41. Hartmann, A., Gleeson, T., Wada, Y. & Wagener, T. Enhanced groundwater recharge rates and altered recharge sensitivity to climate variability through subsurface heterogeneity. *Proc. Natl. Acad. Sci.* **114**, 2842–2847 (2017).

42. Del Grosso, S. et al. Global potential net primary production predicted from vegetation class, precipitation, and temperature. *Ecology* **89**, 2117–2126 (2008).

43. Gedney, N. et al. Detection of a direct carbon dioxide effect in continental river runoff records. *Nature* **439**, 835–838 (2006).

44. Gandois, L., Perrin, A.-S. & Probst, A. Impact of nitrogenous fertiliser-induced proton release on cultivated soils with contrasting carbonate contents: a column experiment. *Geochim. Cosmochim. Acta* **75**, 1185–1198 (2011).

45. Torres, M. A., Moosdorf, N., Hartmann, J., Adkins, J. F. & West, A. J. Glacial weathering, sulfide oxidation, and global carbon cycle feedbacks. *Proc. Natl. Acad. Sci.* **114**, 8716–8721 (2017).

46. Covington, M. D. et al. Carbonates in the critical zone. *Earths Future* **11**, e2022EF002765 (2023).

47. Li, S.-L., Calmels, D., Han, G., Gaillardet, J. & Liu, C.-Q. Sulfuric acid as an agent of carbonate weathering constrained by δ13CDIC: examples from Southwest China. *Earth Planet. Sci. Lett.* **270**, 189–199 (2008).

48. Jiang, Z. et al. Bedrock geochemistry influences vegetation growth by regulating the regolith water-holding capacity. *Nat. Commun.* **11**, 2392 (2020).

49. Zeng, S., Jiang, Y. & Liu, Z. Assessment of climate impacts on the karst-related carbon sink in SW China using MPD and GIS. *Glob. Planet. Change* **144**, 171–181 (2016).

50. Jiang, Z., Lian, Y. & Qin, X. Rocky desertification in Southwest China: impacts, causes, and restoration. *Earth-Sci. Rev.* **132**, 1–12 (2014).

51. Dreybrodt, W., Gabrovšek, F. & Romanov, D. *Processes of a Speleogenesis: A Modeling Approach*. (Karst Research Institute ZRC SAZU, 2005).

52. Gwiazda, R. H. & Broecker, W. S. The separate and combined effects of temperature, soil p CO$_2$, and organic acidity on silicate weathering in the soil environment: formulation of a model and results. *Glob. Biogeochem. Cycles* **8**, 141–155 (1994).

53. Raich, J. W. & Nadelhoffer, K. J. Belowground carbon allocation in forest ecosystems: global trends. *Ecology* **70**, 1346–1354 (1989).

54. Salvatier, J., Wiecki, T. V. & Fonnesbeck, C. Probabilistic programming in Python using PyMC3. *PeerJ. Comput. Sci.* **2**, e55 (2016).

55. Zeng, S., Liu, Z. & Groves, C. Large-scale CO$_2$ removal by enhanced carbonate weathering from changes in land-use practices. *Earth-Sci. Rev.* **225**, 103915 (2022).

56. Liu, Z., Dreybrodt, W. & Liu, H. Atmospheric CO2 sink: silicate weathering or carbonate weathering? *Appl. Geochem.* **26**, S292–S294 (2011).

57. Chen, B. et al. Coupled control of land uses and aquatic biological processes on the diurnal hydrochemical variations in the five ponds at the Shawan karst test site, China: implications for the carbonate weathering-related carbon sink. *Chem. Geol.* **456**, 58–71 (2017).

Author contributions

S.Z. and Z.L. conceived and designed the study. S.Z., Z.L., M.Z., H.S., H. H., M.S., and L.S. performed the simulations and analyzed the data. Y.J., N.G., and Y.Y. contributed to reviewing and editing the paper. S.Z. and Z.L. secured funding for the study. All the authors read and approved the final version of the paper.

Competing interests

Additional information